Lawrence Berkeley National Laboratory
Recent Work

Title
Perfect 2-d Quadrupole Fields From Permanent Magnets

Permalink
https://escholarship.org/uc/item/5g64j97n

Author
Lee, E.P.

Publication Date
1996-04-17

eScholarship.org Powered by the California Digital Library
University of California

LBL-38430
UC-419

Lawrence Berkeley Laboratory
UNIVERSITY OF CALIFORNIA

Accelerator & Fusion
Research Division

Perfect 2-d Quadrupole Fields From Permanent Magnets

E.P. Lee and M. Vella

April 1996

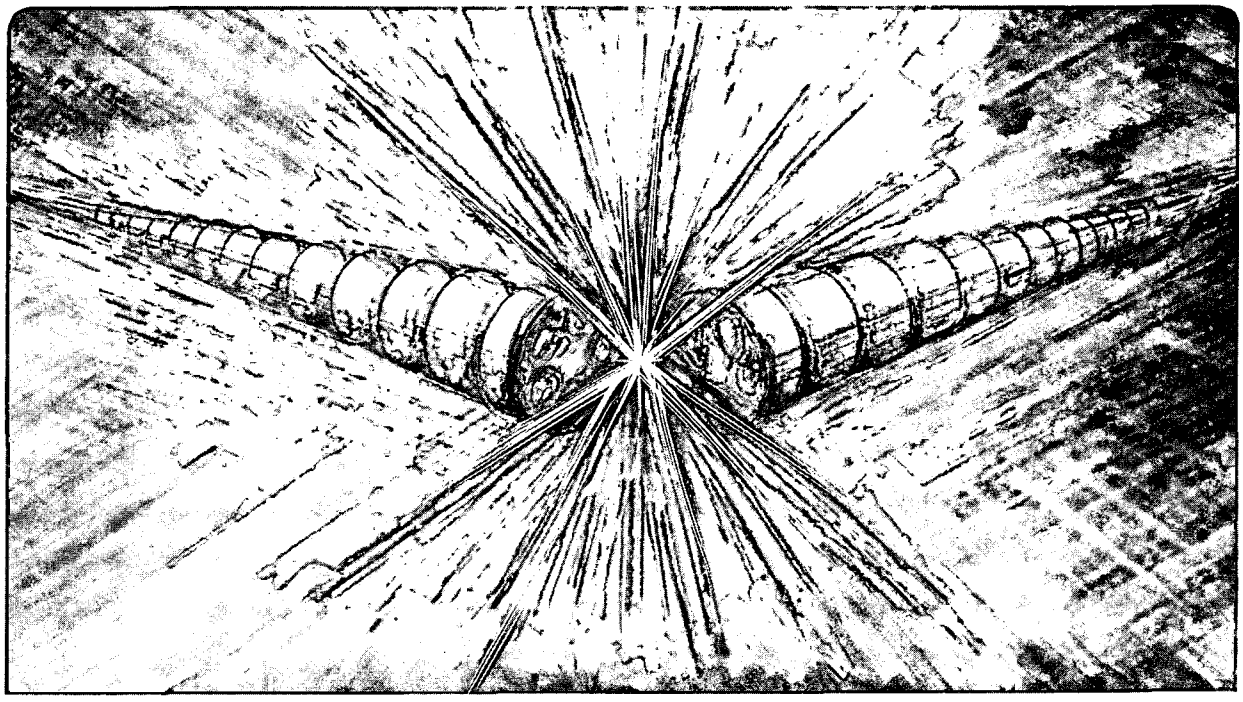

REFERENCE COPY
Does Not
Circulate
Bldg. 50 Library.
LBL-38430
Copy 1

Prepared for the U.S. Department of Energy under Contract Number DE-AC03-76SF00098

DISCLAIMER

This document was prepared as an account of work sponsored by the United States Government. While this document is believed to contain correct information, neither the United States Government nor any agency thereof, nor the Regents of the University of California, nor any of their employees, makes any warranty, express or implied, or assumes any legal responsibility for the accuracy, completeness, or usefulness of any information, apparatus, product, or process disclosed, or represents that its use would not infringe privately owned rights. Reference herein to any specific commercial product, process, or service by its trade name, trademark, manufacturer, or otherwise, does not necessarily constitute or imply its endorsement, recommendation, or favoring by the United States Government or any agency thereof, or the Regents of the University of California. The views and opinions of authors expressed herein do not necessarily state or reflect those of the United States Government or any agency thereof or the Regents of the University of California.

LBL-38430
UC-419
HIFAN 804

Perfect 2-d Quadrupole Fields From Permanent Magnets

Edward P. Lee and Michael Vella

Accelerator and Fusion Research Division
Ernest Orlando Lawrence Berkeley National Laboratory
University of California
Berkeley, California 94720

April 1996

This work was supported by the Director, Office of Energy Research, Office of Fusion Energy, of the U.S. Department of Energy under Contract No. DE-AC03-76SF00098.

LBL-38430
HIFAN 804

Perfect 2-d Quadrupole Fields From Permanent Magnets

Edward P. Lee, Michael Vella

April 1996

Consider the 13-beam channel array shown in Figure 1. It is asserted that, under mathematically ideal assumptions, a pure quadrupole field is centered in each of the 13 beam channel boxes. An identical quadrupole field (for $\bar{H}$, not $\bar{B}$) is also centered in each of the 4 boxes containing 4 magnetic wedges located near the center of the system. An iron yoke ($\mu = \infty$) with the displayed zig-zag shape provides a boundary condition ($H_{\|} = 0$) that makes the 13 channels equivalent to a portion of an infinite array. A similar array can be readily drawn for any number of beams. The quadrupole gradient in the beam channels is $B' = M_0/2b$, where M_0 is the remnant field of the magnetic wedges, and the channel diameter (wedge-to-wedge) is 2b. Note that a unit cell of the array, containing one beam, has diameter $2\sqrt{2}$ b (viewed from a 45° tilt) so its area is 8 b^2. A significant advantage of this design over those using dipolar blocks is the large fraction of cross section devoted to beam channels (50% vs 25%).

Contents:

Ideal Field Structure

We initially assume there is no demagnetization of the magnetic wedges by the opposed $\bar{H}$ field; this is justified for high quality SmCo or Nd B Fe blocks due to the relatively low fields in this configuration (|H| is less than ~ 50% of the remnant field) and permeability close to unity. All fields are given in units of Tesla so μ_0 is suppressed:

$$\bar{B} = \bar{H} + \bar{M}, \tag{1}$$

where $\bar{M} = \pm M_0$ ($\hat{e}_x$ or $\hat{e}_y$) in the wedges. In the iron $\bar{H}$ vanishes, so $\bar{M} = \bar{B}$ there. A more realistic model for the magnetization allows constant permeability in the wedges; if the easy axis is in the + $\hat{e}_x$ direction then

$$\bar{M} = M_0\,\hat{e}_x + (\mu_{//} - 1)\,H_x\hat{e}_x + (\mu_{\perp} - 1)\,H_y\hat{e}_y, \tag{2}$$

and similarly for the easy axis in other directions. If isotropic permeability ($\mu = \mu_{//} = \mu_{\perp}$) is included in the field calculation the advertised ideal field structure for $\bar{H}$ is again

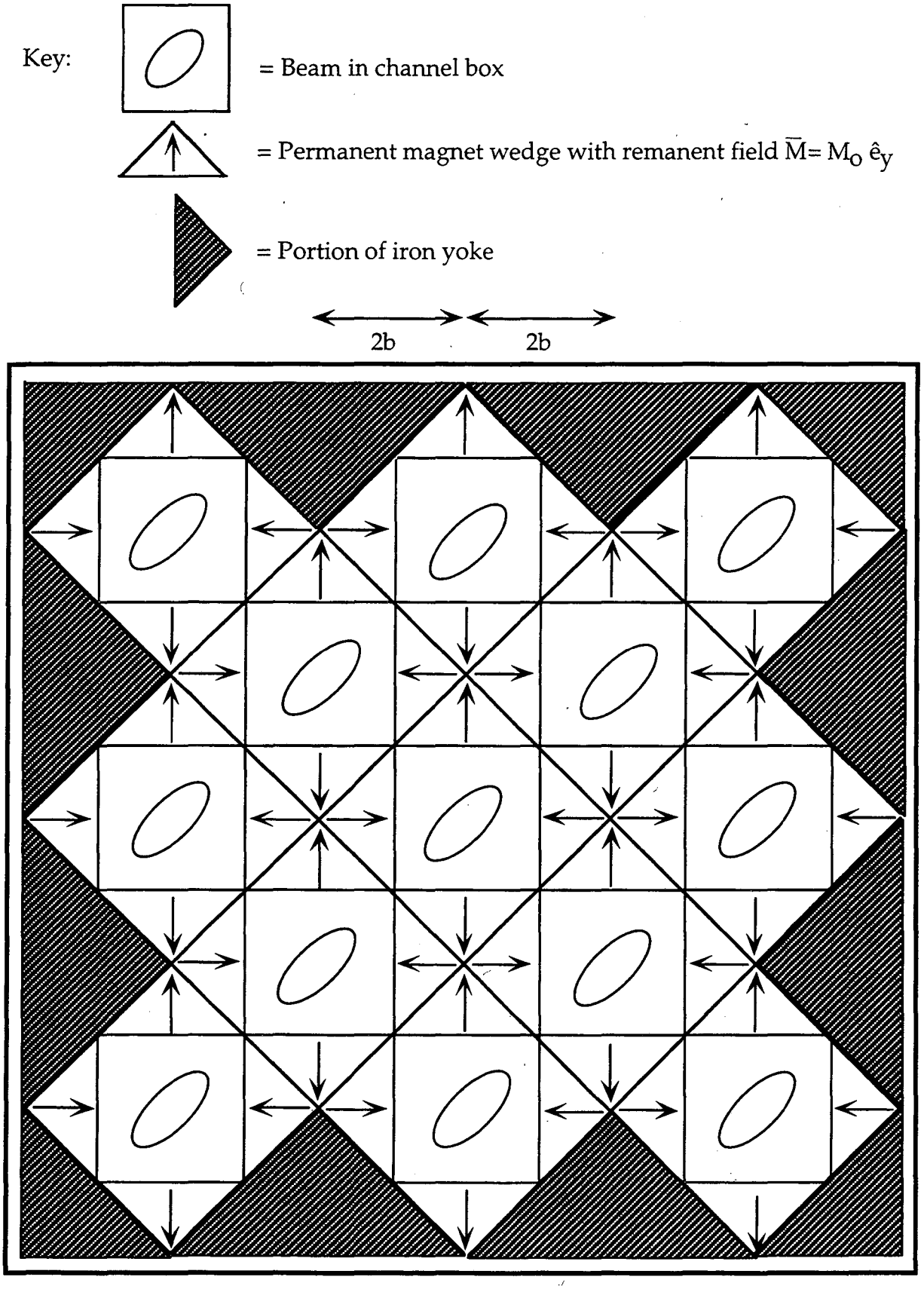

Figure 1
13 Beam Channel Array

present in both the vacuum and magnetic wedge boxes. However, the magnitude of $\bar{H}$ is reduced by the factor $\left[1+(\mu-1)/2\right]^{-1}$. Typically, hard magnetic materials have, $\mu_{\perp} \leq \mu_{//}$ and analytic calculation of fields is considerably complicated by this model feature. However it is found, in this case, that an ideal quadrupole field can be produced in the vacuum boxes by inserting iron wedges along the ± 45° diagonals between the magnetic wedges. Both the vacuum aperture and field strength are reduced by the presence of the additional iron.

Since there are no "true" currents

$$\bar{\nabla} \times \bar{H} = 0, \tag{3}$$

and we are able to use a scalar potential everywhere:

$$\bar{H} = \bar{\nabla} \Phi. \tag{4}$$

From $\bar{\nabla} \bullet \bar{B} = 0$, we have,

$$\nabla^2 \Phi = - \bar{\nabla} \bullet \bar{M}. \tag{5}$$

This equation is completely general and is valid in 3-d as well as 2-d. We assume channels which are much longer than their diameter, so fringe fields can be ignored* ; we only will solve the 2-d equation

$$\left(\frac{\partial^2}{\partial x^2} + \frac{\partial^2}{\partial y^2}\right)\Phi = - \left(\frac{\partial M_x}{\partial x} + \frac{\partial M_y}{\partial y}\right). \tag{6}$$

For a box of 4 magnetic wedges, $\bar{\nabla} \bullet \bar{M}$ is non-zero only on the vertical and horizontal boundaries. It vanishes on the ±45° diagonal interfaces between wedges because lines of $\bar{M}$ flux do not end there; they only kink. This feature is also easily demonstrated mathematically, and its utility for design was previously exploited by Don Swenson in a 1982 LANL memorandum on multiple beam channels. See Figure 2 for a clarification of this discussion. It is found that

Horizontal surfaces $\quad \bar{\nabla} \bullet \bar{M} = M_0 \cdot$ delta function,

Vertical surfaces $\quad \bar{\nabla} \bullet \bar{M} = -M_0 \cdot$ delta function.

* For a calculation of fringe fields see: E. Lee, LBL-38333, HIFAN 801, April 1996.

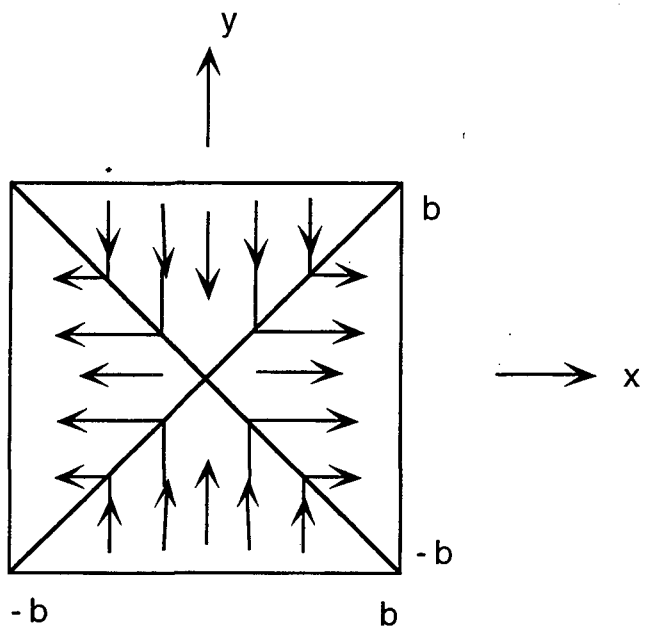

Figure 2

Lines of $\overline{M}$ flux in a box of 4 magnetic wedges. Note that $\overline{\nabla} \bullet \overline{M} = 0$ in the interior of each magnet wedge group because the interfaces are at ±45°. Only on the box surface is $\overline{\nabla} \bullet \overline{M} \neq 0$.

In the example of Figure 2:

$$\overline{\nabla} \bullet \overline{M} = M_O \left[-\delta(x-b) - \delta(x+b) + \delta(y-b) + \delta(y+b)\right]. \qquad (7)$$

A 90° rotation of an entire infinite array around any channel or 4-wedge box center causes $\Phi \rightarrow -\Phi$. Hence we have the expansion around any box center

$$\Phi = \Phi_0 + \Phi_2 r^2 \cos 2\theta + \Phi_6 r^6 \cos 6\theta + \Phi_{10} r^{10} \cos 10\theta \quad +... \qquad (8)$$

We have asserted that $\Phi_6 = \Phi_{10} = ... = 0$ inside the box. We can also set $\Phi = 0$ at all box centers, so only the quadrupole term Φ_2 would remain. This is the result of the system symmetry and the condition
$\oint \overline{H} \bullet \overline{d\ell} = 0$ around any closed loop.

We now assume the advertised result of identical pure quadruple ($\overline{H}$) fields centered in all boxes (vacuum and block boxes) and show that it satisfies the jump/boundary conditions. It is sufficient to examine the three adjacent boxes shown in Figure 3. The scalar potential is assumed to have the form:

box #	box center	assumed potential in box
#1	x=o y=o	$\Phi^{(1)} = A\left[x^2 - y^2\right]$ $\left(= A\, r^2 \cos 2\theta\right)$
#2	x=2b y=o	$\Phi^{(2)} = A\left[(x-2b)^2 - y^2\right]$
#3	x=2b y=2b	$\Phi^{(3)} = A\left[(x-2b)^2 - (y-2b)^2\right]$

Recalling the fundamental equation for Φ:

$$\left(\frac{\partial^2}{\partial x^2} + \frac{\partial^2}{\partial y^2}\right) \Phi = - \left(\frac{\partial Mx}{\partial x} + \frac{\partial My}{\partial y}\right), \tag{9}$$

it is clear that we have a solution inside each box, where $\overline{\nabla} \bullet \overline{M} = 0$. We need only to verify that $H_X = \partial\Phi/\partial x$ and $H_Y = \partial\Phi/\partial y$ are continuous across the horizontal and vertical box interfaces respectively, and H_X and H_Y jump by $\pm M_O$ at the vertical and horizontal interfaces respectively. Continuity of the parallel components is built into their assumed form, e.g. at the vertical interface at x = b, between boxes #1 and #2 we have

$$\Phi^{(1)} = \Phi^{(2)} = A\left(b^2 - y^2\right), \tag{10}$$

$$Hy = \frac{\partial\Phi}{\partial y} = - 2Ay \tag{11}$$

on both sides. Continuity of H_X between boxes #2 and #3 is similarly guaranteed. For the normal component of $\overline{H}$ at the box #1/box #2 interface we have

$$(-2Ab) - (2Ab) = H_x^{(2)} - H_x^{(1)} = - \int_{b-}^{b+} dx \frac{\partial M_x}{\partial x} = M_o, \tag{12}$$

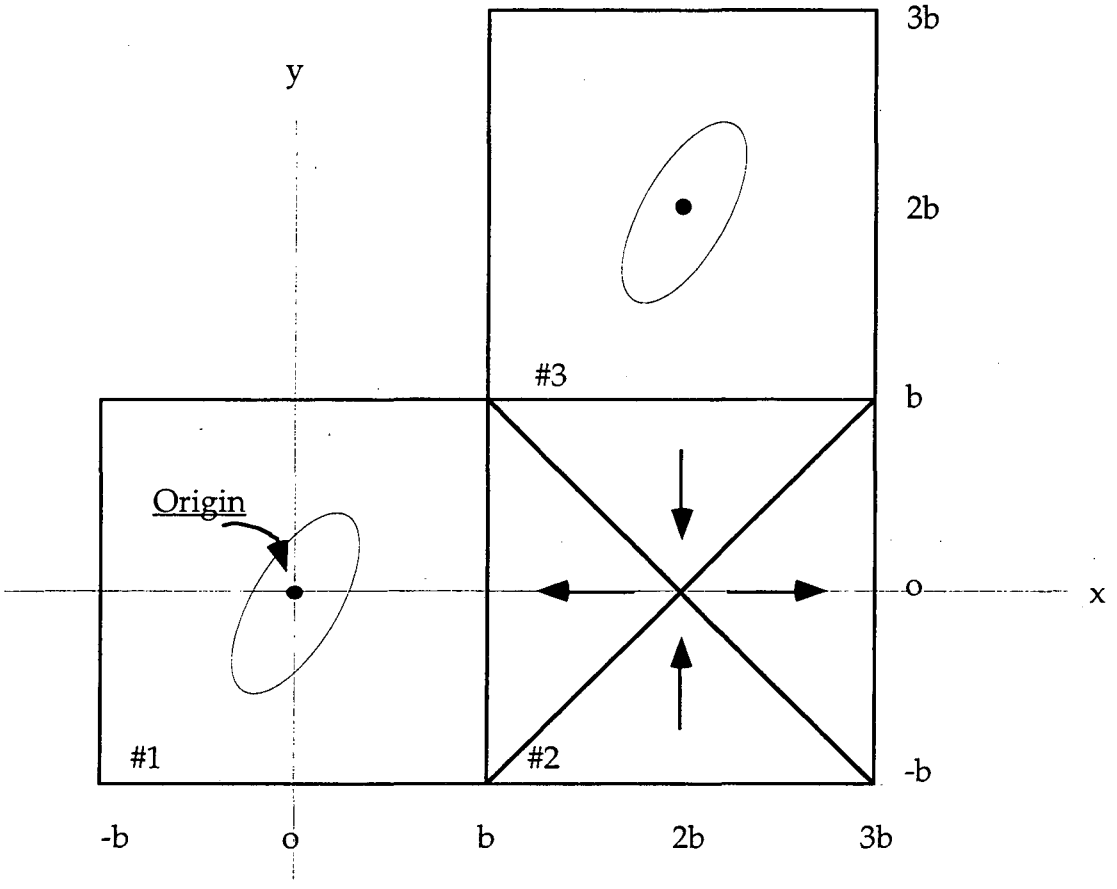

Figure 3

Layout of three adjacent boxes for application of jump conditions on $\overline{H}$.

yielding

$$A = -\frac{M_o}{4b}. \tag{13}$$

Similarly at the box #2/box #3 interface

$$(2Ab) - (-2Ab) = -\int_{b-}^{b+} dy \frac{\partial M_y}{\partial y} = -M_o, \tag{14}$$

which is again satisfied by

$$A = -\frac{M_o}{4b}. \tag{15}$$

The assumed solution is therefore consistent in an infinite array with the value of A derived above.

We have, centered in each beam channel box,

$$\Phi = -\frac{M_o}{4b}\left(x^2 - y^2\right), \tag{16}$$

$$B_x = H_x = \frac{\partial \Phi}{\partial x} = -\frac{M_o}{2b} x, \tag{17}$$

$$B_y = H_y = \frac{\partial \Phi}{\partial y} = \frac{M_o}{2b} y, \tag{18}$$

$$B' = \left|\frac{\partial B_x}{\partial x}\right| = \frac{M_o}{2b}. \tag{19}$$

It has been shown that Φ is a simple quadrupole potential centered in the 4-wedge boxes as well as in the channel boxes. Therefore $\bar{H}$ is normal to the diagonal interfaces between wedges. For the finite system iron* replaced wedges on diagonal surfaces around the edge exactly where the tangent $\bar{H}$ field would vanish in the infinite array. This is a sufficient condition to leave fields unperturbed in the wedges and channels since the essential property of iron ($\mu = \infty$) is to eliminate the tangential component of $\bar{H}$ on its surface.

* In the simulation of the finite system described in the last section of this report, magnetic steel with $\mu \approx 80$ is placed on these surfaces.

Application To A Heavy Ion Fusion Driver

The following example suggests that permanent magnet channels can efficiently transport driver scale currents at high energy, but with an appreciable penalty in quadrupole length (and at present, cost) compared with superconducting arrays.

Let the magnetic wedge material be Nd B Fe, with remnant magnetization $M_o \approx 1.2$ T and $\mu = 1.0$. Questions of radiation damage, etc. are put off for future study. Transportable current per unit area of the array is maximized* by choosing b = 0.036 m, independent of M_o, so we get the very modest quadrupole gradient

$$B' = \frac{M_o}{2b} = \frac{1.2\,T}{2\times.036} = 16.7\,T/m. \qquad (20)$$

By contrast, gradients in the range 20 – 60 T/m are typical for superconducting layouts for HIF drivers.

To get a 4.0 MJ driver we accelerate 800 μC of Cs^+ to 5.0 GeV. A typical lattice parameter set is obtained for the intermediate energy 1.0 GeV:

Ion = Cs^+,

A = 132.9 amu, q = +1,

Kinetic energy T=1.00 GeV,

Number of beams N = 36,

$$\frac{v}{c} = \beta = \sqrt{\frac{2T}{Mc^2}} = \sqrt{\frac{2\times 1.0}{132.9\times 0.9315}} = 0.127, \qquad (21)$$

$$\text{Ion rigidity} = B\rho = 3.107\frac{\beta A}{q} = 3.107\times 0.127\times\frac{132.9}{1.0} = 52.5\,T-m, \qquad (22)$$

$$\text{Quad strength} = K = \frac{B'}{B\rho} = \frac{16.7}{52.5} = 0.318\,m^{-2}. \qquad (23)$$

Assuming field occupancy fraction η=.5 and undepressed tune $\sigma_o = 72°$, then the half period length is†

---

* See note on optimum aperture at end of this section.

† For transport formulas see HIFAR Note #425 and HIFAN Report #701.

$$L = \left[\frac{2(1-\cos\sigma_o)}{(\eta K)^2\left(1-\frac{2}{3}\eta\right)}\right]^{\frac{1}{4}} = 3.01\,\text{m}. \tag{24}$$

We have set b = .036 m = distance from a beam center to a wedge. Suppose the vacuum aperture (d) is at .034 m and the maximum beam edge radius is given by the standard (for heavy ion fusion) allowance

$$a = \frac{d - .01\,\text{m}}{1.25} = .0192\,\text{m}. \tag{25}$$

The mean beam edge radius is then

$$\bar{a} = \frac{a}{1+\frac{\eta K L^2}{4}\left(1-\frac{\eta}{2}\right)} = \frac{.0192}{1+\frac{0.5\times 0.318\times(3.01)^2\times 0.75}{4}} = 0.0151\,\text{m}. \tag{26}$$

The maximum transportable beam perveance is (emittance = 0)

$$Q = \left(\frac{\bar{a}}{2L}\right)^2 2(1-\cos\sigma_o) = \left(\frac{0.0151}{2\text{ x }3.01}\right)^2 \times 2 \times (1-\cos 72) = 8.71\times 10^{-6}. \tag{27}$$

Transportable line charge density per channel is given by

$$\lambda = (4\pi\epsilon_o)\left(\frac{T}{qe}\right)Q = \frac{1}{9\times 10^9}\times\frac{10^9}{1.0}\times 8.71\times 10^{-6} = 0.968\frac{\mu C}{m}. \tag{28}$$

Since 800μC is divided among N=36 beams, we have a pulse length

$$\ell_p = \frac{\text{total charge}}{N\lambda} = \frac{800}{36\times 0.968} = 23.0\,\text{m}, \tag{29}$$

and pulse duration is

$$t_p = \frac{\ell_p}{\beta c} = \frac{23.0}{0.127\times 3\times 10^8} = 0.602\,\mu\text{s}. \tag{30}$$

The 36 beam square array has diameter (including iron)

$$\text{diameter} = \underset{\text{(boxes)}}{6\times 2\sqrt{2}b} + \underset{\text{(iron)}}{2\sqrt{2}b} = 14\sqrt{2}\times 0.036 = 0.713\,\text{m}. \tag{31}$$

The above numbers are not unreasonable. The big change with respect to superconducting magnets is the low B' (by a factor of ~3), which is compensated by increasing η by a similar factor. This leaves less room per half period for acceleration and probably results in a longer accelerator. On the other hand, cryogenics, thermal insulation, power supplies, leads, superconducting cable, magnet end configuration, and high field mechanical stresses are eliminated. Cost may be a problem. At a current price of about $\$5/cm^3$ for finished blocks* , we have a total cost (per lattice half period of 3.01 m):

$$\text{cost of blocks} = N\eta L(2b)^2 \times (5 \times 10^6\ \$/m^3) = 36 \times 0.5 \times 3.01 \times (.072)^2 \times \$5 \times 10^6 = 1.4\ M\$,$$

which is .47 M$/m of linac. Clearly a significant reduction in unit price is needed to make this an attractive option for a driver. However, it may be acceptable in a scaled experimental system.

Note on optimum channel size

A frequently used figure of merit (FOM) for transport is total beam current divided by total cross sectional area associated with the focusing lenses. For a multibeam transport structure this FOM is the current per beam divided by the unit cell area. While a global cost minimum may not exactly coincide with this FOM, it does provide a useful starting point for design.

Note that at any given energy the current is proportional to the beam perveance:

$$I \alpha Q, \tag{32}$$

and the unit cell area is proportioned to the squared magnetic block distance ($8b^2$ in the present case). Hence

$$\text{FOM} \quad \alpha \quad \frac{Q}{b^2}. \tag{33}$$

Maximum transportable Q is proportional to $(a/L)^2$ with σ_o fixed at its stable maximum ($\sigma_o \lesssim 90°$):

$$Q \quad \alpha \quad \left(\frac{a}{L}\right)^2. \tag{34}$$

The square of the lattice half period length is, for given σ_o and η, inversely proportional to K and therefore proportional to b:

$$L^2 \quad \alpha \quad \frac{1}{K} = \frac{B\rho}{B'} = \left(\frac{2b}{Mo}\right)(B\rho) \quad \alpha \quad b. \tag{35}$$

* Private communication: S. Lund of LLNL has recently received a vendor quote close to this figure.

For the relation between beam edge radius a and block distance b, we adopt the traditional standard clearance for image and alignment related effects and add another 2.0 mm for structure between the beam pipe aperture and magnet block:

$$b = \underset{\text{extra structure}}{0.002\text{ m}} + \underset{\text{image allowance}}{1.25a} + \underset{\text{alignment allowance}}{0.01\text{ m}} .$$

Equivently a=0.8 (b–0.012).

Putting together the pieces we have

$$\text{FOM} \;\alpha\; \frac{Q}{b^2} \;\alpha\; \frac{1}{b^2}\left(\frac{a}{L}\right)^2 \;\alpha\; \frac{(b-0.012)^2}{b^3}. \tag{36}$$

The maximum FOM follows from

$$0 = \frac{d}{db}(\text{FOM}) \;\alpha\; \frac{2(b-0.012)}{b^3} - \frac{3(b-0.012)^2}{b^4}, \tag{37}$$

which is solved by

$$b_{optimum} = 3 \times 0.012 = 0.036\text{ m}. \tag{38}$$

More generally we may write

$$b_{optimum} = 3 \times \left(\underset{\text{structure}}{\text{extra}} + \underset{\text{allowance}}{\text{alignment}}\right). \tag{39}$$

We note here that if the extra structure allowance is increased from 0.002 m to 0.01 m, the optimum b is increased to 0.06 m. A linac transporting the same total current then uses ~22 beams and the cost for magnetized blocks is increased from 0.47 M$/m to 0.79M$/m of linac. A different design approach is found if it is assumed that beam steering or magnet shimming can eliminate the need for a large alignment allowance. In this case b may be made very small, with a simultaneous large increase in number of beams to produce larger transported currents per unit area than were found above.

The wedge–based system we have described has one magnetic wedge set per beam channel; this is a very efficient use of space and material. For comparison it is interesting to consider a system made up of simple dipolar blocks instead of the wedge sets. It is then found that (for given M_o, b, and η) the quadrupole gradient is increased by a factor of 1.18, and the number of beams is decreased by this factor. However; two dipole blocks per beam channel are required, so the mass of blocks and their cost per meter of linac is increased by a factor of 2/1.18 = 1.7. In addition, the dipole block system contains idle

spaces equal in number to the beam channels resulting in a significant increase in total cross sectional area of the array (also by a factor of 1.7).

2-D Simulation Ideal Magnetic Quadrupole Arrays

Ideal permanent magnet quadrupoles were simulated using the Opera-2d/Tosca finite element magnetostatic code. First, a single cell in an infinite array was simulated, and the results are compared here with analytic predictions for the infinite array limit. A comparison with an array constructed of simple dipole blocks is also made. Second, the practical utility of the ideal quadrupole configuration is illustrated by simulating a thirteen beam array with an iron boundary of large but finite permeability.

Infinite Array with Ideal Magnetic Wedges

The magnetic field lines of an octant of an ideal magnetic quadrupole cell in an infinite array are illustrated in Figure 4a by plotting lines of the magnetic field $(\bar{B})$. In this and all following simulation examples, each full cell is square, with width 4b = 0.24 m, so in the ideal array it would contain two beams. The octant in Figure 4 shows octants of two beam channels because this is the smallest simulation segment allowed by symmetry. The easy axes of the magnets are illustrated by arrows. For comparison with theory, special magnetic material properties were created by using a linear B-H curve, with $\mu = 1$, B_r (i.e., M_o) = 1.120 T, and H_c = -1.120 T. The quadrupole field gradient of the simulated channel was found by taking Fourier moments of the tangential magnetic field along arcs with radii between 0.01 m and 0.059 m. The simulated gradient was found to be 9.3331 T/m, which agrees very well with the analytic prediction of 1.1200/(2 x 0.06) = 9.3333 T/m. For this and all other simulations reported here, Opera's quadratic mesh option was used to achieve an internal tracking error < 0.5%. The quadratic mesh option refines the mesh by adding nodes at the midpoint of each of the specified mesh lines; the added nodes are connected with straight line sections. The quadratic option refines the mesh but reduces the size of output files by saving only end point data for the hard mesh nodes. In this example all the higher order moments were < 1E-4 for cases with constant $\mu \neq 1$, also in agreement with theory. For the case $\mu = 1$, the un-normalized moments* for the m = 5 and 9 poles were about 10^{-5} T at a radius of 0.059 cm, compared with 0.5506 T for m=1. This is much less than the nominal accuracy of this simulation. So, the higher order moments were found to be zero within the accuracy of this simulation, and the ideal nature of this quadrupole geometry is confirmed.

---

* For Opera-2d/Tosca output the moment designation (m = 1, 5, 9, ..) denotes the power of r in the magnetic field multipole rather than the corresponding magnetic potential (2, 6, 10, ..) The value of the moment is the strength of the multipole field component at a particular value of r. Simulation fields are expressed in Gauss and radii in centimeters.

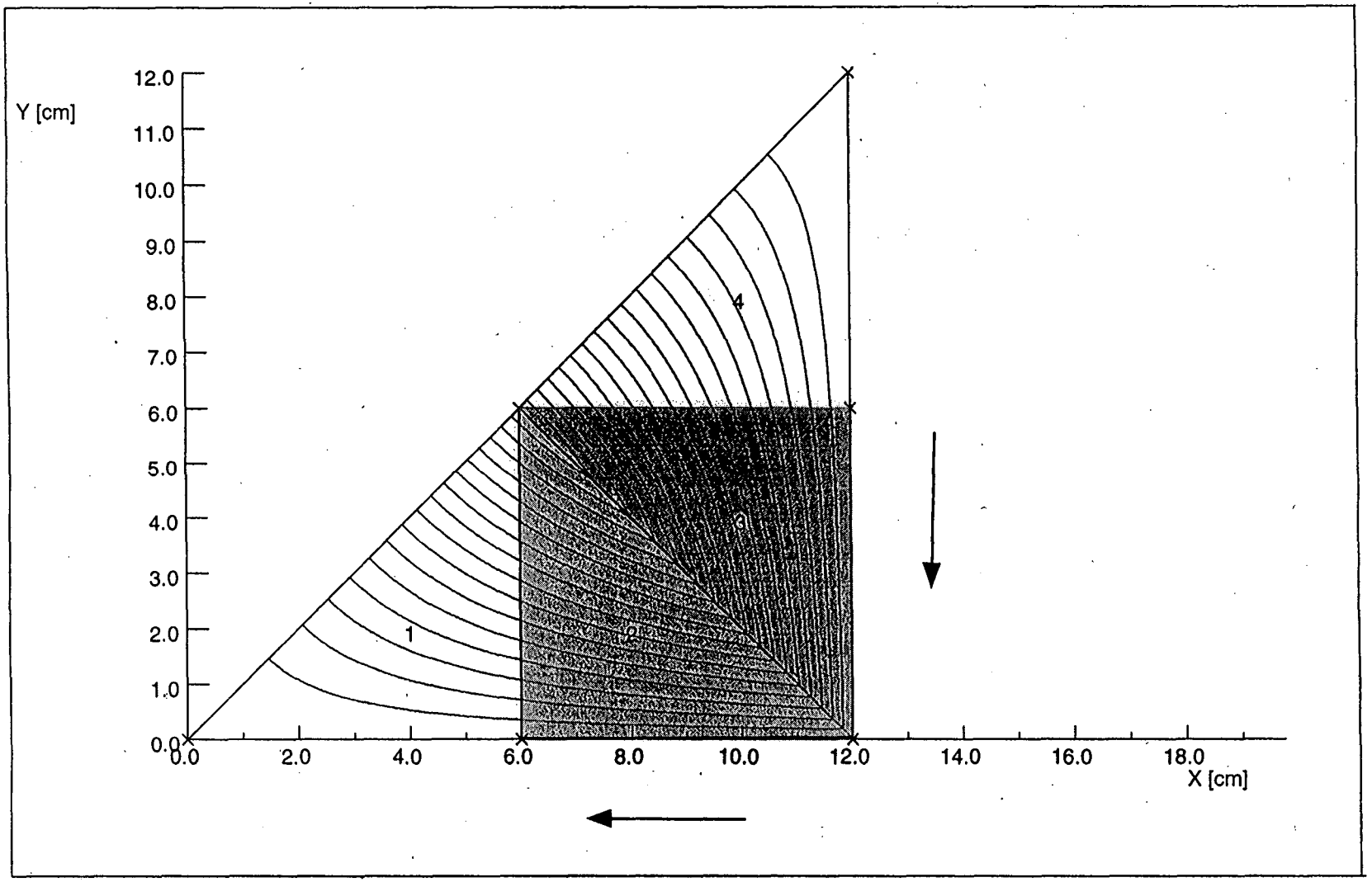

Figure 4a

An octant of a cell of an infinite array of ideal permanent magnet quadrupoles was simulated with Opera-2d. In an ideal quadrupole array, the smallest-simulation region allowed by symmetry contains octants of two beam channels. (a) Magnetic field lines are plotted.

The ideal nature of this configuration is illustrated graphically by plotting |B| (called BMOD in Opera) contours in Figure 4b. The "bulls eye" pattern of evenly spaced, circular BMOD contours graphically confirms a uniform, symmetric magnetic gradient centered in the channel. Since higher order multipole moments also have higher order asymmetries, the presence of finite higher order moments would produce non-circular |B| contours, as will be illustrated in later examples. As mentioned previously, an interesting theoretical characteristic of this ideal quadrupole geometry is that $\bar{H}$ forms perfect quadrupoles both in the beam channels and inside the magnets, as illustrated in Figure 4c.

For comparison with the ideal array, a standard dipole block quadrupole cell in an infinite array was simulated using the same B-H characteristics as above, μ = 1, B_r (i.e., M_o) = 1.120 T, and H_c = -1.120 T. Magnetic field lines for an octant of this cell are illustrated in Figure 5a, and |B| contours are shown in Figure 5b. The most obvious difference between an ideal quadrupole and a standard dipole block array is that an ideal quadrupole array has double the number of beam channels per magnet block. From Figure 5, only the lower section in the dipole based array is usable for beam transport, because the upper section contains an octopole field in lowest order and is typically occupied by a non-magnetic spacer. This gives the ideal quadrupole array an intrinsic scaling advantage. From Figure 4, the ideal quadrupole array also produces high quality quadrupoles in both lower and upper non-magnet sections.

The geometric advantage of an ideal quadrupole array is somewhat diminished by its' lower quadrupole field gradient. For the examples illustrated in Figures 4 and 5, the gradient of the ideal quadrupole is 9.33 T/m, compared with 11.01 T/m for the dipole block array, i.e., the ideal quadrupole produces 15% less gradient. However, field quality for the ideal array is intrinsically better, since the dipole array has a finite dodecapole moment, that creates significant magnetic perturbations beyond a radius of 0.05 m. The presence of higher order moments in the dipole array is visually confirmed by asymmetries in the |B| contours of Figure 5b.

For ideal quadrupoles fabricated from real materials, a subtle systematic issue arises regarding treatment of the magnetic permeability in the direction orthogonal to the easy axis. Only a few hard magnetic materials are approximately linear through the entire range $H_C < H$, and even fewer have the same permeability parallel and perpendicular to the easy axis, i.e., usually $\mu_{parallel} > \mu_{perp}$. A difference between the two permeabilities can generate small higher order moments in an ideal quadrupole, which would otherwise be perfect. This effect might not be noticed in a dipole based array, because the dipole geometry has much larger intrinsic higher order moments. The 1995 version of Opera-2d/Tosca was used for this work. For hard, non-linear materials, this version self-consistently finds the appropriate $\mu_{parallel}$ for the B-H range of interest, but blindly takes μ_{perp} from the slope of the B-H curve at the intercept to the horizontal axis, i.e., at B=0. This can give rise to very large (incorrect) values of μ_{perp} for highly nonlinear material. Given nonlinear B-H data, Opera-2d's ad hoc treatment of $\mu_{parallel}$ and μ_{perp} can generate small higher order multipoles in an ideal quadrupole array. This is

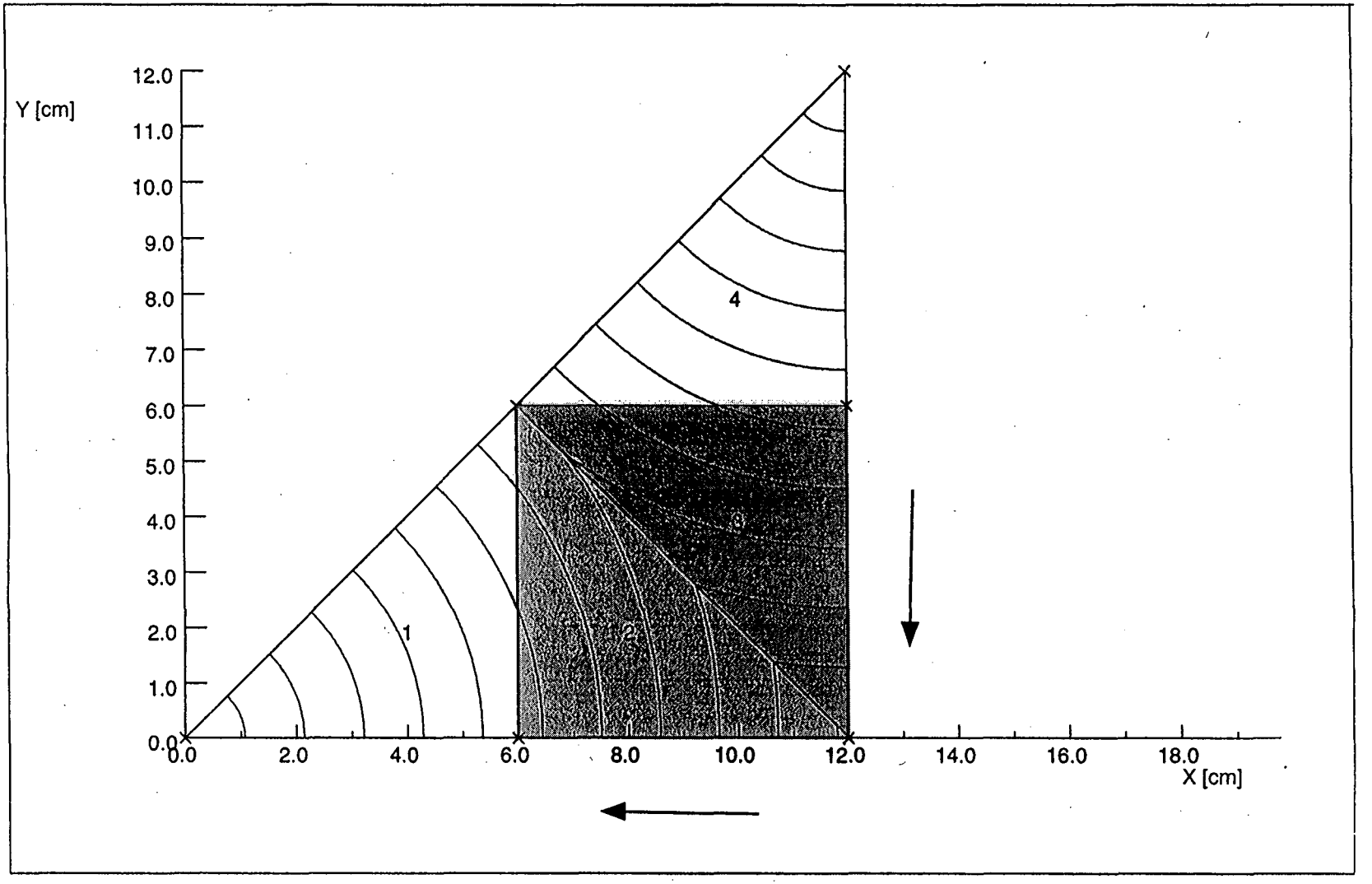

Figure 4b

An octant of a cell of an infinite array of ideal permanent magnet quadrupoles was simulated with Opera-2d. In an ideal quadrupole array, the smallest simulation region allowed by symmetry contains octants of two beam channels. (b) |B| contours take the shape of evenly spaced, concentric circles, which indicates that the gradient is dominated by the linear, quadrupole field, component.

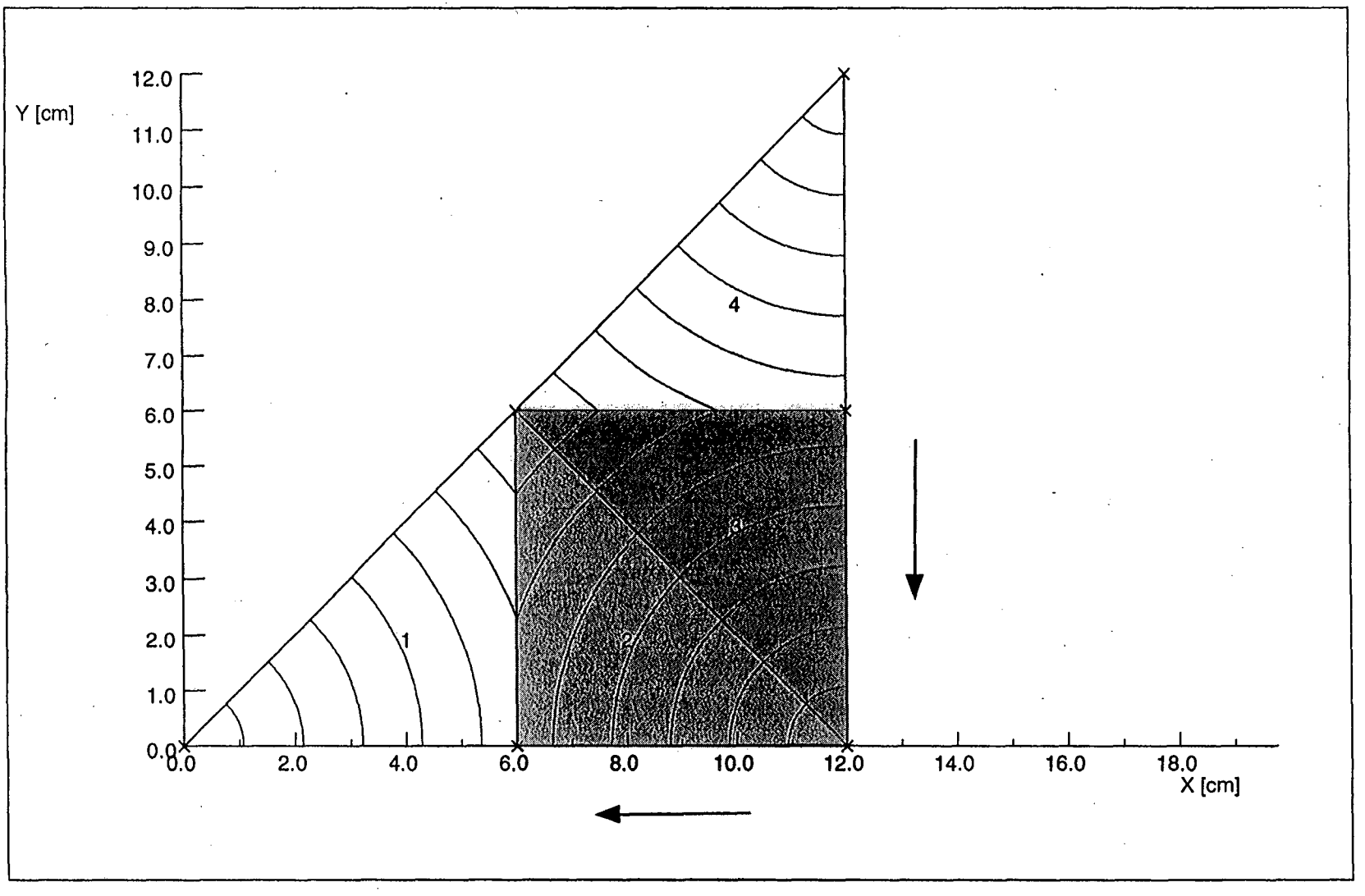

Figure 4c

An octant of a cell of an infinite array of ideal permanent magnet quadrupoles was simulated with Opera-2d. In an ideal quadrupole array, the smallest simulation region allowed by symmetry contains octants of two beam channels. (c) In ideal quadrupoles, the |H| contours everywhere have the shape of evenly spaced, concentric circles. In this example, $\mu = 1.0$.

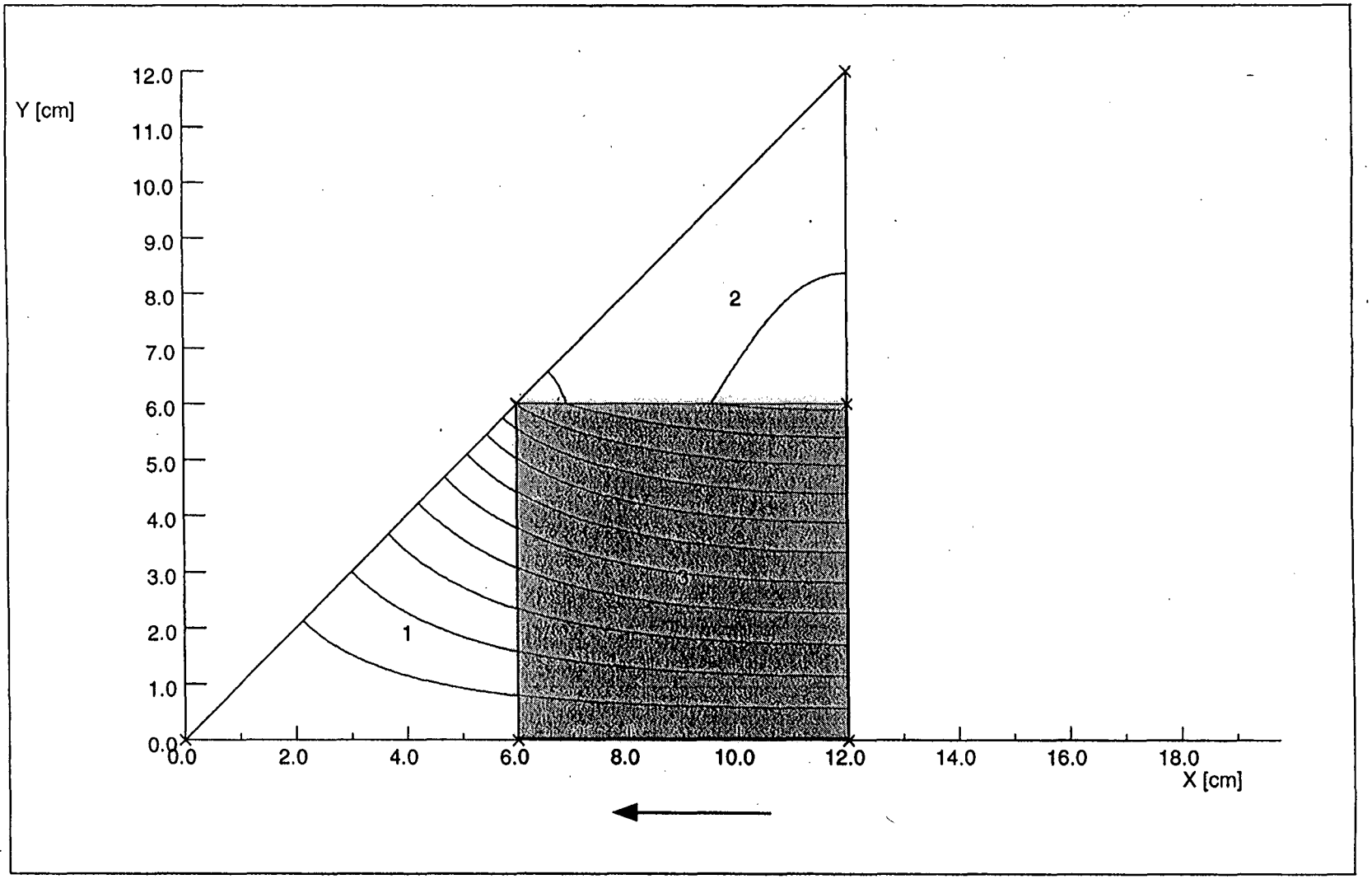

Figure 5a

An octant of a cell of an infinite array of dipole block quadrupoles was simulated with Opera-2d. The smallest simulation region allowed by symmetry contains only one beam channel. Magnetic field lines are plotted

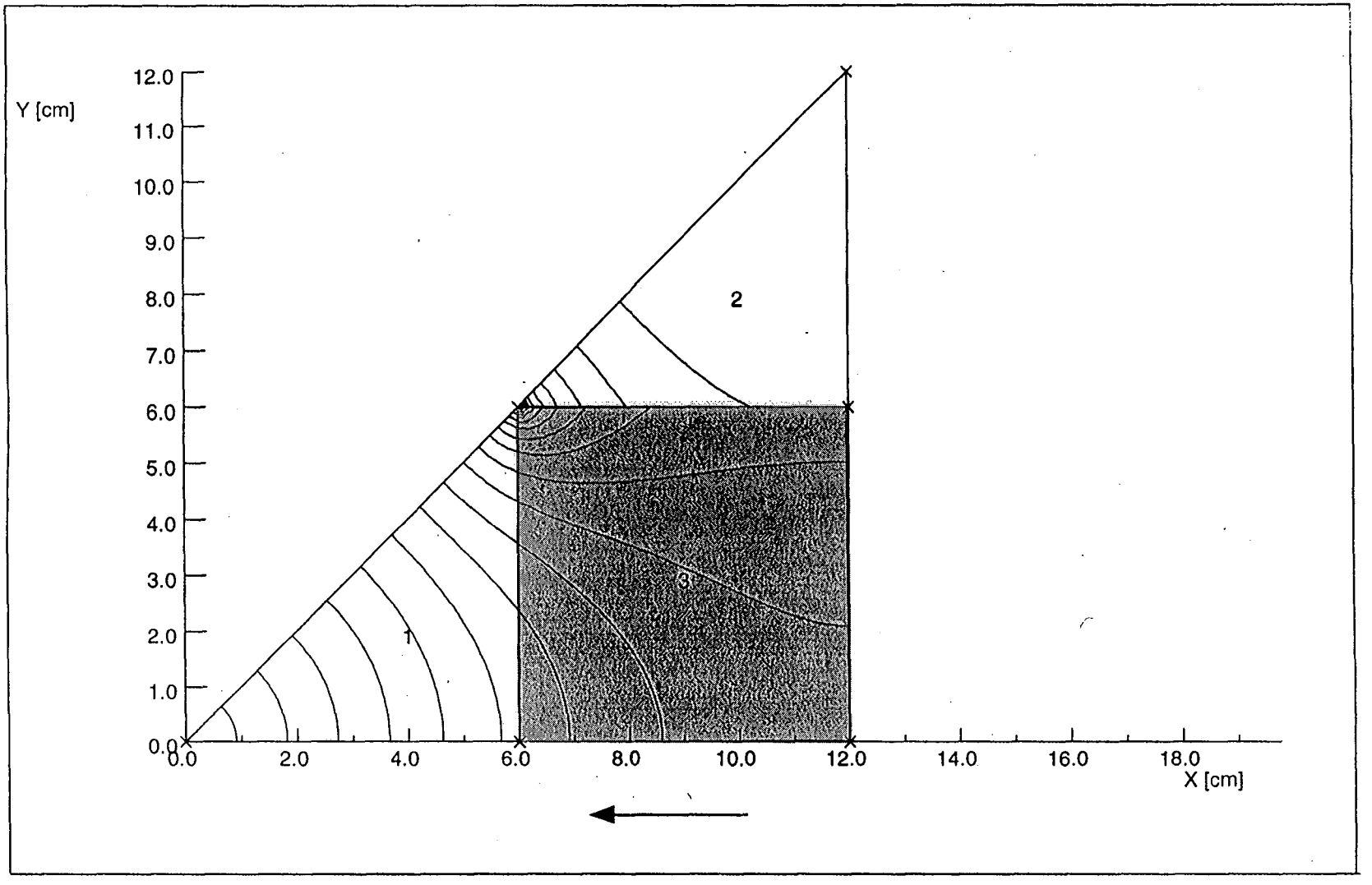

Figure 5b

An octant of a cell of an infinite array of dipole block quadrupoles was simulated with Opera-2d. The smallest simulation region allowed by symmetry contains only one beam channel. |B| contours deviate from evenly spaced concentric circles, indicating the presence of higher order multipole components. In this example, $\mu = 1.0$.

illustrated in Table 1, where moments have been tabulated for three cases of B-H data: (1.) $\mu = 1$; (2.) nonlinear μ; and (3.) linear NdFeB (maximum B-H). The nonlinear B-H data has an effective $\mu_{parallel} = 1.03$, and $\mu_{perp} = 1.57$. This produces a 4.5% lower quadropole gradient than would be for $\mu = 1$, and an order of magnitude increase in the dodecapole field moment (m=5). Since the same mesh was used in these examples, with the same nominal computational error, the increased dodecapole moment is attributed to the higher effective μ_{perp} forced by the code. For the case of $\mu = 1$ the dodecapole moment is entirely attributed to numerical inaccuracy. This hypothesis is also supported by the results for the third case, which used linear B-H data generated from the B_r and H_c typical of NdFeB. In this case, $\mu_{parallel} = \mu_{perp} = 1.039$, and the simulation gradient essentially equals that predicted by the finite μ theoretical results. The three sets of B-H data are shown in Table 2. It should be noted that the present version of Opera-3d allows operator control of anisotropic magnetic properties, and the 1996 release of Opera-2d is expected to include an anisotropic magnetic option.

Finite Array

An octant of the thirteen beam array shown in Figure 1 was simulated with realistic magnetic steel B-H data, appropriate symmetry boundary conditions on two sides, and finite boundary on one side, as illustrated in Figure 6a. The finite boundary along the steel side necessitated a large mesh. Magnetic materials properties were prescribed by using B-H data for tenten stainless steel ($\mu \approx 80$), and linear NdFeB permanent magnets, with $B_r = 13.3$ kG and $H_c = -12.8$ kG as listed in Table 2 (c, d). The quadratic option was used to reduce Opera's internal rms tracking error to < 0.5%.

The "ideal" nature of the quadrupoles in the 13 channel array was confirmed in several ways. A plot of the magnetic field lines is shown in Figure 6b, and constant absolute values of the magnetic field $|B|$ are plotted in Figure 6c. The bulls eye patterns of the $|B|$ plots visually indicate that high quality quadrupole fields are produced in each channel, and that they are geometrically centered. The magnetic centers were confirmed within 0.01cm of the geometric centers by reading out BMOD along the x- and y-axes.

Each quadrupole channel in the array was also quantitatively characterized by using Opera's moments package to take the Fourier moments of the tangential component of the magnetic field along a series of arcs centered at the geometric center of each channel. The moments were taken for arcs of radii, r = 1, 3, 4, and 5 cm. The results are tabulated in Table 3. For every channel, the nonvanishing higher order m = 5 and m = 9 moments were order 1E-7 compared with computed quadrupole moment; this is zero within the accuracy of this simulation. Therefore, the conclusion is that this 13 beam array effectively has no higher order moments in the two dimensional limit despite the non-ideal characteristics of the steel.

Table 1. Fourier moments of the magnetic field tangent to an arc are shown for radii of 1.0 cm in a beam channel in an infinite array. The standard deviation of the moments for the quadrupole gradient (m = 1) was << 1E-5. The standard deviation of the non-vanishing higher order moments, m = 5 and 9, was comparable to the computed moments, indicating that indicated higher order moments are due to finite mesh errors. The finite m = 5 moment for the nonlinear material is attributed to the large, incorrect, value of μ_{perp}, extracted from the B-H data.

NORMALIZED MOMENTS (av @ r=1, 5, 5.9 cm)

	bh data	mu	Br	Hc	Opera-2d m=1	Theory m=1, theory	Opera-2d m=5	Opera-2d m=9
ideal quad	ed1.bh	1	11,200	-11,200	933.31	933.33	-4.53E-05	-1.31E-07
dipole quad	ed1.bh	1	11,200	-11,200	1101.59		4.70E-02	4.84E-06
ideal quad	ndfebo.bh	nonlin	11,200	-9,814	891.23		3.68E-04	-1.61E-07
dipole quad	ndfebo.bh	nonlin	11,200	-9,814	1068.42		4.93E-02	5.09E-06
nonlinear, μ parallel = 1.03, μperp = 1.57								
ideal quad	ed5.bh	1.04	13,300	-12,800	1087.08	1086.60	-3.02E-05	-4.02E-08
dipole quad	ed5.bh	1.04	13,300	-12,800	1288.70		5.66E-02	5.88E-06

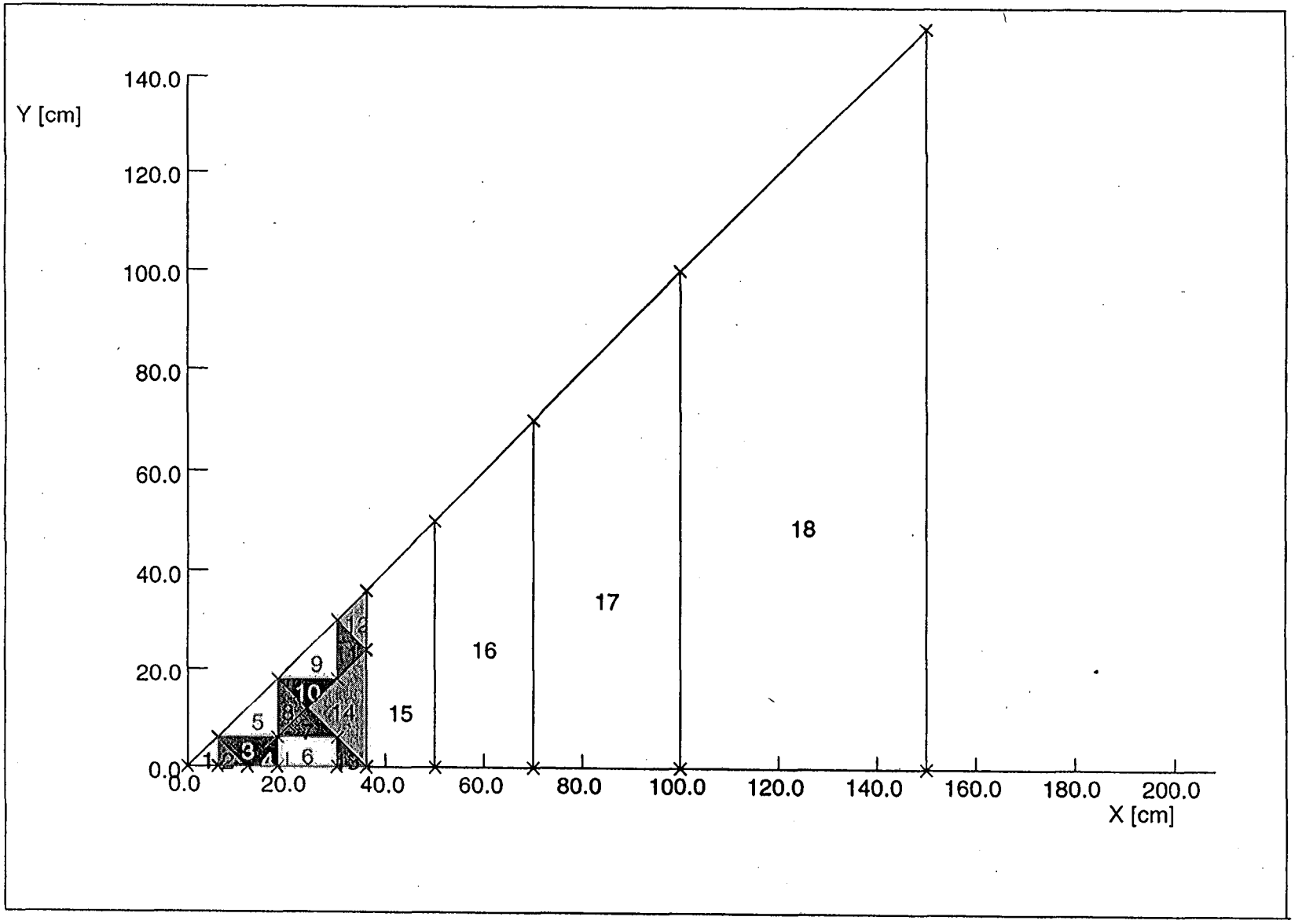

Figure 6a

An octant of a thirteen beam array of ideal quadrupoles with a magnetic steel boundary was simulated with Opera-2d. The size of the mesh and boundary conditions are illustrated.

Table 2. B-H data used in Opera-2d simulations: (a) Linear, $\mu = 1$; (b) Nonlinear, μ parallel $\cong$ 1.03, μperp $\cong$ 1.57; (c) Linear NdFeBO, $\mu = 1.039$; (d) Data for magnetic steel.

(a) Linear, $\mu = 1$.

H, Gauss	B, Gauss
-11200	0
-10200	1000
-9200	2000
-7200	4000
-5200	6000
-3200	8000
-1200	10000
0	11200

(b) Nonlinear, μ parallel = 1.03 and μperp = 1.57.

B	H
0	-9814.34
1000	-9198.58
2000	-8482.30
3000	-7652.92
4000	-6798.41
6000	-4963.72
8000	-3078.76
10000	-1156.11
11200	0.0

(c) Linear NdFeBO, $\mu = 1.039$.

B	H
0	-12800.0
1000	-11837.0
2000	-10875.0
4000	-8950.3
6000	-7025.5
8000	-5100.7
10000	-3175.9
12000	-1251.1
13300	0

(d) Tenten magnetic stainless steel

B	H
0	0.0000
6400	79.5775
9200	135.2820
10100	159.1550
11000	190.9860
12000	238.7320
13000	318.3100
14000	493.3800
14500	644.5780
15000	875.3520
15500	1273.2400
15750	1591.5500
16000	2148.5900
16500	3342.2500
17000	4774.6500
17500	6525.3500
18000	9151.4100
18500	11936.6000
19000	15119.7000
19500	18541.6000

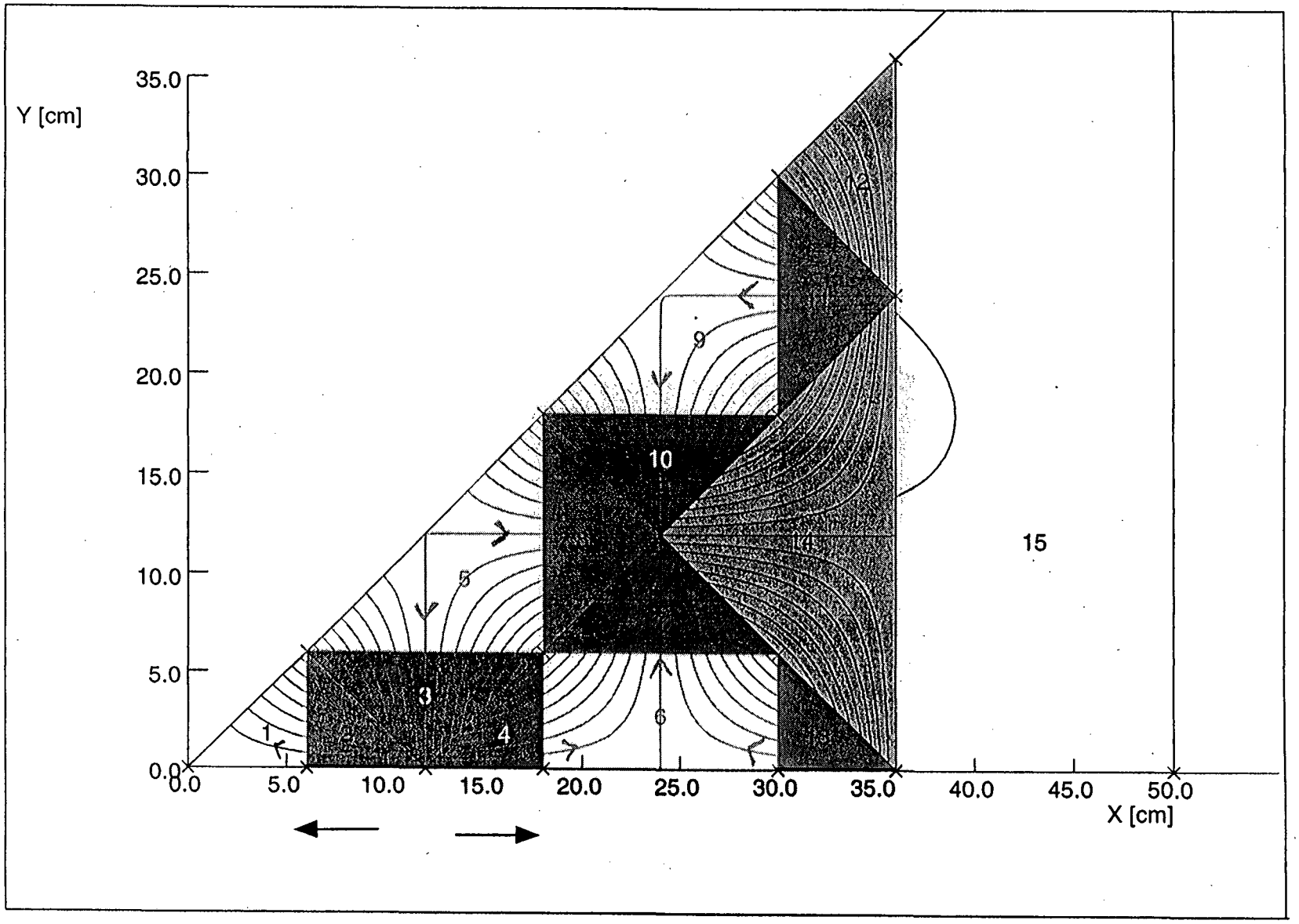

Figure 6b

An octant of a thirteen beam array of ideal quadrupoles with a magnetic steel boundary was simulated with Opera-2d. Magnetic field lines are plotted. Note that essentially no flux leaks from the iron. The only line outside the iron corresponds to the zero magnetic potential line.

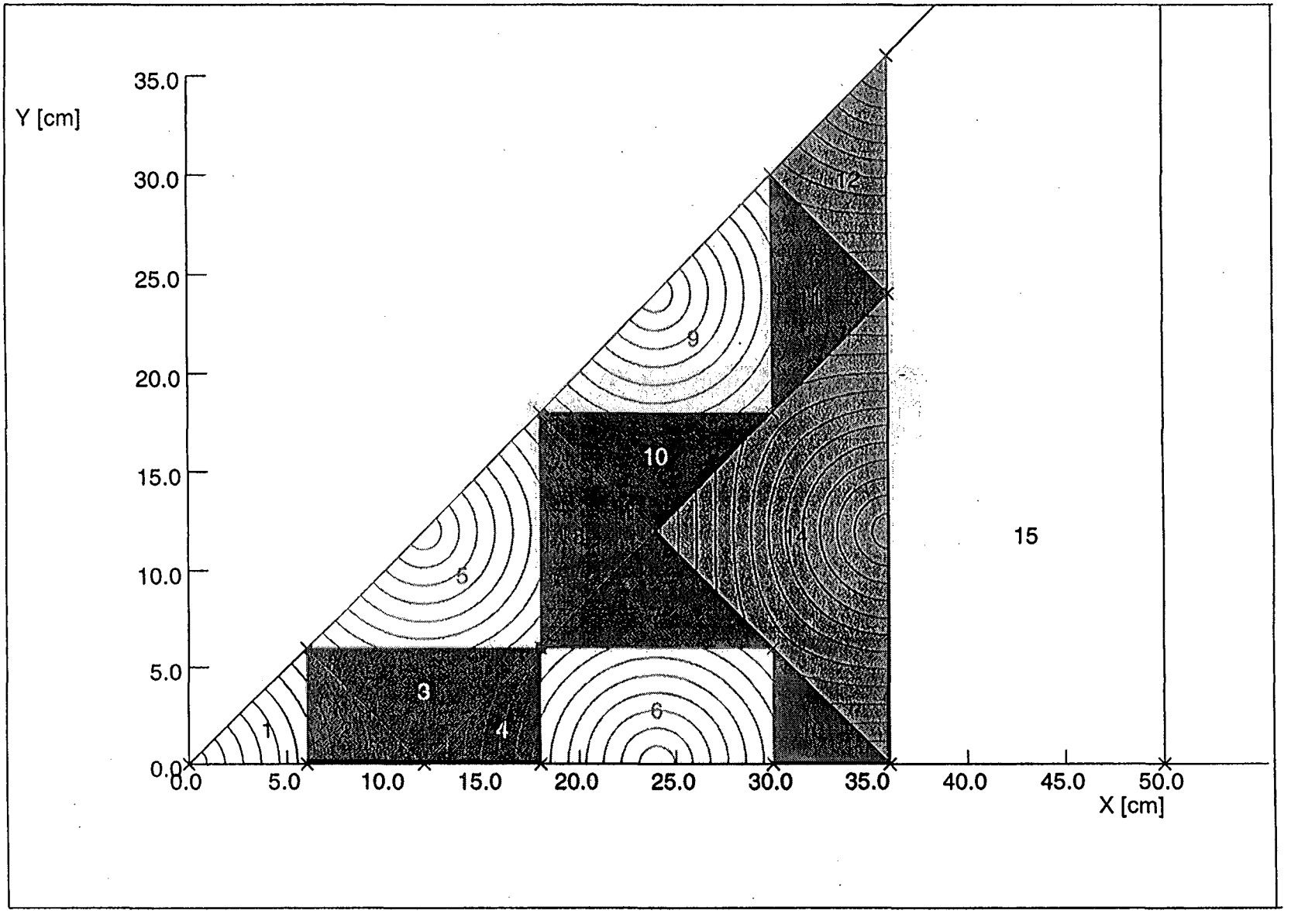

Figure 6c

An octant of a thirteen beam array of ideal quadrupoles with a magnetic steel boundary was simulated with Opera-2d. |B| contours take the shape of evenly spaced, concentric circles, which indicates that the gradient is dominated by the linear, quadrupole field, component. The |B| centers appear to coincide with the geometric beam centers. In this example, $\mu = 1.039$, $B_r = 13.3$ kG and $H_c = -12.8$ kO

Table 3. Fourier moments of the magnetic field tangent to an arc are shown for radii of 1, 3, 4, and 5 cm. The arcs were centered at the geometric center of each channel in an octant of a thirteen beam array with a steel boundary. All moments are normalized with respect to radius, i.e. divided by r, r^5, or r^9. Only the nonvanishing higher order moments are shown, m = 5, 9; and these are zero within the accuracy of this simulation. Magnetic properties were specified by using linearized B-H data generated from B_r and H_c of NdFeB with $\mu = 1.039$.

NORMALIZED MOMENTS

center	r, cm	m=1	m=5	m=9
0, 0	1	1087.11		
	3	1087.11	-3.06E-04	-3.80E-06
	4	1087.11	-9.69E-05	-3.77E-07
	5	1087.11	-3.94E-05	-6.38E-08
12, 12	1	1087.11		
	3	1087.53	-1.25E-03	2.98E-06
	4	1087.46	-3.12E-04	9.76E-08
	5	1087.41	-1.11E-04	-5.84E-09
24, 24	1	1087.11		
	3	1086.50	2.22E-04	-7.50E-06
	4	1086.54	4.52E-05	-6.60E-07
	5	1086.57	1.42E-05	-1.03E-07
24, 0	1	1087.11		
	3	1086.56	-4.32E-04	-4.43E-06
	4	1086.60	-1.43E-04	-3.98E-07
	5	1086.61	-3.78E-05	-6.68E-08
	average	1086.97	-2.04E-04	-1.19E-06
	stdev	0.35	3.75E-04	2.75E-06

The computed moments correspond to the coeficients of B_θ in the Fourier expansion with θ:

$$B_\theta = M_1(r) \sin \theta + M_5(r) \sin 5\,\theta + M_9(r) \sin 9\,\theta + \ldots, \tag{40}$$

with $M_1 \propto r$, $M_5 \propto r^5$, etc. expected in vacuum in the limit of perfect computational accuracy. The predicted (ideal) value at r = 1.0 cm

$$M_1 = \frac{(B_r)^{r}/_{b}}{2\left(1+\frac{\mu-1}{2}\right)} = 1087.1 \tag{41}$$

is in excellent agreement with the simulation average = 1086.97.

LAWRENCE BERKELEY NATIONAL LABORATORY
UNIVERSITY OF CALIFORNIA
TECHNICAL & ELECTRONIC INFORMATION DEPARTMENT
BERKELEY, CALIFORNIA 94720